ECS Transactions, 86 (6) 69-74 (2018)
10.1149/08606.0069ecst ©The Electrochemical Society

Layer Control of 2D-MoS_2 by Atomic Layer Etching and Its Device Characteristics

K. S. Kim[a], K. H. Kim[a], Y. J. Ji[a], and G. Y. Yeom[a,b]

[a] School of Advanced Materials Science and Engineering, Sungkyunkwan University, 2066 Seobu-ro, Jangan-gu, Suwon-si, Gyeonggi-do 16419, Republic of Korea.
[b] SKKU Advanced Institute of Nano Technology (SAINT), Sungkyunkwan University, 2066 Seobu-ro, Jangan-gu, Suwon-si, Gyeonggi-do 16419, Republic of Korea.

Molybdenum disulfide (MoS_2) has been intensively investigated due to its unique properties in various electronic and optoelectronic applications with different band-gap energies from 1.29 to 1.9 eV as the number of layers is decreased. To control the MoS_2 layers, atomic layer etching (ALE) composed of a Cl radical adsorption step and a reacted-compound desorption step via a low-energy Ar^+-ion exposure can be a highly effective technique to avoid damage and contamination that occur during the cyclic steps. In this presentation, MoS_2 ALE is compared with conventional plasma etching, and the MoS_2-ALE mechanism is reported with the results of an experiment and a simulation. Especially, using the ALE method, mono-layer/bi-layer MoS_2 field effect transistors (FETs) were fabricated and their electrical characteristics were investigated and compared with the MoS_2 FETs fabricated with pristine mono-layer/bi-layer MoS_2. In addition, mono-/multi-layer lateral-heterojunction device was fabricated using the ALE technique after photoresist patterning of multi-layer MoS_2.

The control of the MoS_2 layers is one of the most important technologies in terms of various nano-device applications; however, difficulty is encountered with the controlling of the layers of MoS_2 when conventional synthetic methods such as chemical vapor deposition (CVD) (1, 2) and plasma-enhanced chemical vapor depostion (PECVD) (3) in addition to the exfoliation method (4) are used. For this reason, various methods have been reported by many research groups for the control of the MoS_2 layers such as Ar plasma etching (5), xenon difluoride (XeF_2) etching (6), laser thining (7), and thermal annealing (8,9), but these methods are ineffective for a layer-by-layer control of the MoS_2 layers at the atomic scale because the control of the MoS_2 layers only depends on the thinning time in addition to the difficulty regarding a processing that does not induce damage. On the contray, aftomic layer etching (ALE) is one of the most important techniques that allows a precise control of the number of MoS_2 layers without inducing damage and contamination through the chemical adsorption and physical desorption of the cyclic steps (10, 11). While the mono-layer of graphene is composed of a one-atom-thick layer, one transition metal dichalcogenides (TMDs) mono-layer is composed of a three-atom-thick layer; therefore, the ALE mechanisms of the two structures are quite different. In this research, the ALE mechanism of a mono-layer MoS_2 from a bi-layer MoS_2 is achieved through a sequential Cl radical adsorption and an Ar^+ ion desorption, is

Downloaded on 2018-12-06 to IP 203.252.59.115 address. Redistribution subject to ECS terms of use (see ecsdl.org/site/terms_use) unless CC License in place (see abstract).

presented. In addition, the possibility of the controlling of the S/Mo ratio of the top MoS_2 layer during the Ar^+ ion desorption step as a function of time is confirmed.

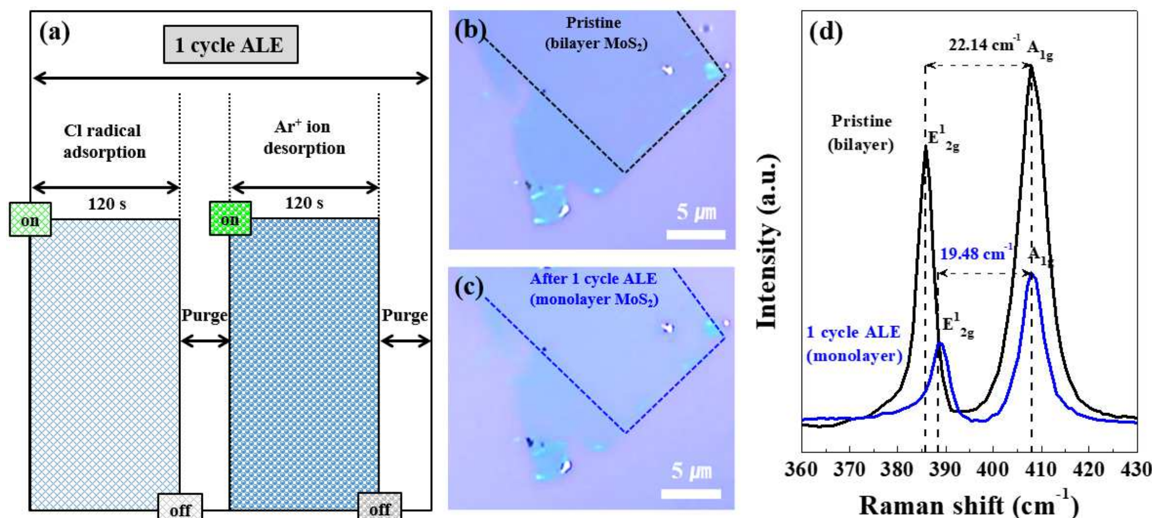

Figure 1. (a) Schematic of the MoS_2 ALE one cycle composed of the Cl radical adsorption step (120 s) and the Ar^+ ion desorption step (120 s). (b), (c) Optical microscopic images of the pristine exfoliated bi- and mono-layer MoS_2 after one ALE cycle. (d) Raman spectroscopic data of the pristine bi- and mono-layer MoS_2 that were observed after the one cycle ALE.

Figure 1(a) shows the schematic of the cyclic etching process composed of sequential reactant adsorption step and reacted compound desorption step for one cycle ALE. Figure 1(b), (c) show the optical microscopic images of (b) the pristine bi-layer MoS_2 and (c) the mono-layer MoS_2 after one cycle of ALE of the bi-layer MoS_2, and Figure 1(d) shows the Raman spectroscopic data of the pristine bi-layer MoS_2 and the mono-layer MoS_2 obtained after the one ALE cycle in Figure 1(a). Through the adsorption of reactive Cl radical on the bi-layer MoS_2 surface for 120 s during the adsorption step and through the following Ar^+ ion exposure with an adequate energy of ~20 eV for 120 s during the desorption step, the mono-layer MoS_2 could be obtained from the bi-layer MoS_2 by one cycle ALE. Therefore, using the ALE, the thickness of the MoS_2 layers could be precisely controlled by the number of etch cycles. In this study, the ALE mechanim of the MoS_2 layers was further investigated.

Downloaded on 2018-12-06 to IP 203.252.59.115 address. Redistribution subject to ECS terms of use (see ecsdl.org/site/terms_use) unless CC License in place (see abstract).

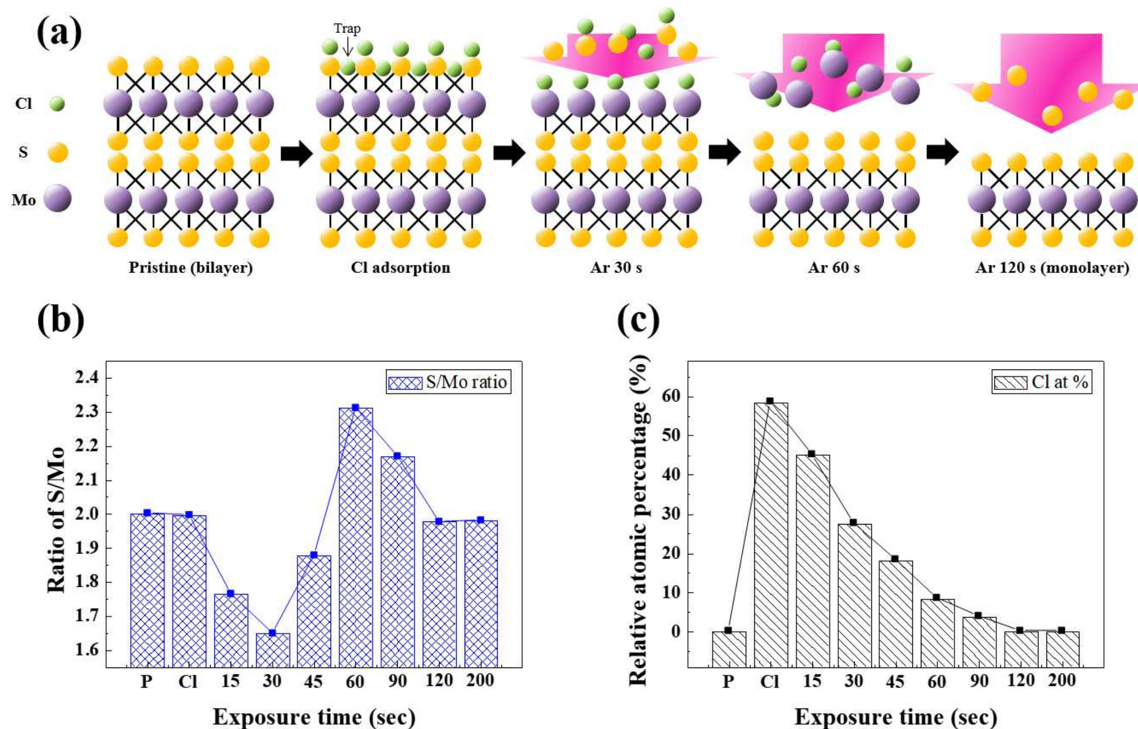

Figure 2. (a) Schematic of the MoS_2 ALE mechanism through the Cl radical adsorption and the Ar^+ ion desorption as a function of exposure time. (b) Change of the S/MO ratio and (c) relative Cl atomic percentage (at %) on the MoS_2 surface using XPS during the ALE of the bi-layer.

Figure 2 shows the schematic diagram of the detailed MoS_2 ALE mechanism for one cycle ALE from a bilayer MoS_2 to one MoS_2 monolayer through Cl radical adsorption and Ar^+ ion desorption. When Cl was adsorbed on the bilayer MoS_2, Cl atoms are adsorbed on the top S atoms of MoS_2 and are also trapped between top S atoms and Mo atoms by the van der Waals force because 6 electrons in the Mo atoms ($4d^5 5s^1$) are fully bound to S atoms. After the Cl radical adsorption, due to the higher electronegativity of Cl compared to S, the binding energy between $S_{(top)}$ and Mo (binding between S $3s^2 3p^4$ and Mo $4d^5 5s^1$) is decreased significantly (the binding energy of top S atoms is decreased from 1.99 to 1.47 eV when estimated by a simulation technique), therefore, during the Ar^+ ion desorption, the top S atoms of the 1st MoS_2 layer are preferentially removed as S-Cl for the Ar^+ ion desorption time of 0 ~ 30 s. After the removal of top S atoms, the trapped Cl atoms form Mo-Cl bonding and the binding energy between Mo atoms and bottom S atoms are also significantly decreased (the binding energy of Mo atoms is decreased from 2.15 to 1.63 eV) and Mo is preferentiall removed also as Mo-Cl for the Ar^+ ion desorption time of 30 ~ 60 s. After the removal of top S and Mo atoms of the 1st MoS_2 layer, only the bottom S atoms bonded with 2nd MoS_2 layer by van der Waals force are remained and their binding energy is also decreased after the removal of Mo atoms (the binding energy of bottom S atoms is decreased 1.91 to 1.5 eV), therefore, bottom S atoms are finally removed during the Ar^+ ion desorption time of 60 ~ 120 s. In our previous work (XPS analysis and simulation calculation), it can be understood that the Mo-Cl bonds are formed under the top S-Cl bonds of top MoS_2 layer due to the trapped Cl atoms and the $S_{(top)}$-Mo-$S_{(bottom)}$ layer is sequentially removed (10). After the

Downloaded on 2018-12-06 to IP 203.252.59.115 address. Redistribution subject to ECS terms of use (see ecsdl.org/site/terms_use) unless CC License in place (see abstract).

120 s of Ar^+ ion exposure time, the fresh 2nd MoS_2 layer (bilayer to monolayer) is exposed, and, due to the low Ar^+ ion desorption energy of 20 eV, the further exposure to Ar^+ ion does not change the exposed MoS_2 monolyer structure after the one cycle MoS_2 ALE. Figure 2(b),(c) show the change in the S/Mo ratio and the relative Cl at % on the MoS_2 surface measured using XPS as a function of Ar^+ ion exposure time (15 ~ 200 s) during the desorption step of MoS_2 ALE after the Cl radical adsorption on the MoS_2 surface for the bilayer MoS_2. As shown, before the exposure to Ar^+ ion after the Cl radical adsorption step for the MoS_2 ALE, the ratio of S/Mo was ~2.0 indicating stoichiometric MoS_2 was not changed even with the Cl radical adsorption of relative at % of ~58 % (The percentage of Cl is high due to Cl atoms trapped between $S_{(top)}$ and Mo). Therefore, it shows that, for the Cl adsorbed MoS_2, the top S atoms will be removed first by the exposure to Ar^+ ions. In addition, during the Cl radical adsorption step, it turned out that Cl atoms can be additionally trapped between top S atoms and mid Mo atoms by van der Waals force. As shown in Figure 2(b),(c), with the increase of Ar^+ ion exposure time from 0 to 30 s, the ratio of S/Mo was decreased gradually from 2 to ~1.6 in addition to the decrease of relative Cl percentage from ~58 to ~27 % due to the preferential removal of the top S atoms bonded to Cl having the lowest binding energy in the top MoS_2 layer. When the Ar^+ ion exposure time was increased from 30 to 60 s, the ratio of S/Mo was increased from ~1.6 to ~2.3 indicating the removal of Mo atoms. The relative Cl percentage was continuously decreasing from 27 % at 30 s to about ~8 % at 90 s indicating the removal of Mo by Mo-Cl. However, when the Ar^+ ion exposrure time was further increased from 60 to 120 s, the ratio of S/Mo was again decreased from ~2.3 to ~2.0 indicating the removal of bottom S atoms after the removal of Mo atoms in the 1st MoS_2 layer. After the removal of Mo in the 1st MoS_2, only bottom S atoms are remaining and the bottom S atoms are preferentially removed by the Ar^+ exposure from 60 to 120 s. The remaining Cl percentage was also decreased to 0 after the Ar^+ ion exposure to 120 s indicating the exposure of the fresh 2nd MoS_2 layer. After the preferential removal of the bottom S atoms, the 2nd MoS_2 layer is exposed but, even though the Ar^+ ion exposure time was extened to 200 s after 1st MoS_2 layer was completely removed at 120 s, the ratio of S/Mo was remaining at ~2 indicating that the 2nd MoS_2 layer was not etched at all by the Ar^+ ion energy of 20 eV.

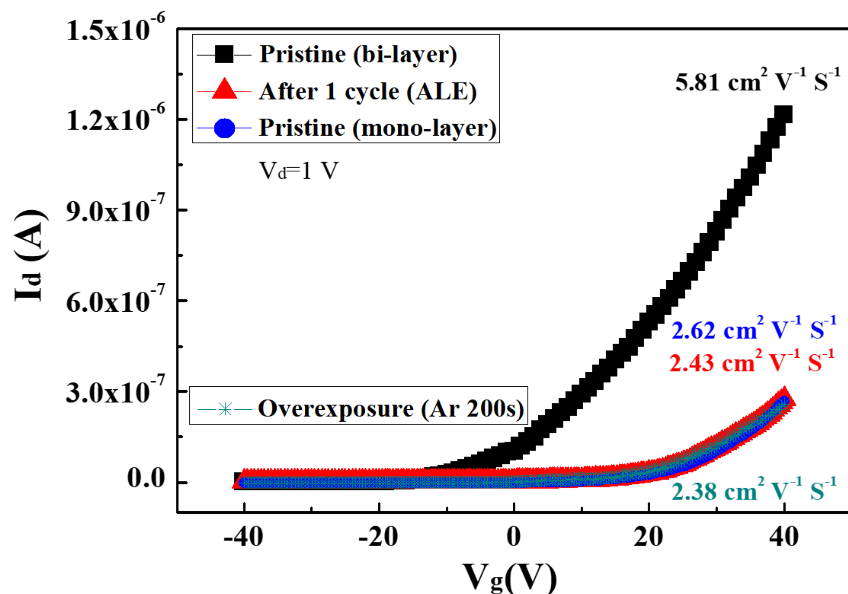

Downloaded on 2018-12-06 to IP 203.252.59.115 address. Redistribution subject to ECS terms of use (see ecsdl.org/site/terms_use) unless CC License in place (see abstract).

Figure 3. Drain currents vs. gate voltages of the bottom-gate MoS_2 FETs that were fabricated with the exfoliated bilayer MoS_2, the exfoliated monolayer MoS_2, the exfoliated bilayer MoS_2 after the 1 cycle MoS_2 ALE, and the overexposure (Ar^+ ion beam, 20 eV from 120 s to 200 s) after the 1 cycle MoS_2 ALE.

To investigate the degree of damage on the monolayer MoS_2 that occured after the etching of the bilayer MoS_2 by the one cycle MoS_2 ALE, bottom-gate MoS_2 FETs were fabricated with the exfoliated pristine bilayer MoS_2, the exfoliated pristine monolayer MoS_2, and the exfoliated monolayer MoS_2 that were obtained using the one cycle MoS_2 ALE of the exfoliated bilayer MoS_2. In the MoS_2-FET fabriation, the exfoliated MoS_2 was used instead of the CVD MoS_2, because the exfoliated MoS_2 layers comprise a stoichiometric and defectless MoS_2. The characteristics of the drain currents vs. the gate voltages (I_d vs. V_g) of the MoS_2 FETs are shown in Figure 3. The MoS_2 FETs that were fabricated with the pristine monolayer and bilayer MoS_2 exhibited the typical electrical characteristics of the MoS_2 FETs. Also, the MoS_2 FET that was fabricated with the monolayer MoS_2 that was obtained after the one cycle MoS_2 ALE of the bilayer MoS_2 and the monolayer MoS_2 overexposed (Ar^+ ion beam, 20 eV from 120 s to 200 s) after the 1 cycle MoS_2 ALE exhibited electrical characteristics that are the same as those that were fabricated with the pristine monolayer MoS_2. The field effect mobility of the exfoliated bilayer MoS_2 (black), the exfoliated monolayer MoS_2 (blue), the exfoliated bilayer MoS_2 after the 1 cycle MoS_2 ALE (red), and the monolayer MoS_2 overexposed after the 1 cycle MoS_2 ALE (green) were estimated to be 5.81, 2.62, 2.43, and 2.38 cm^2 V^{-1} s^{-1}, respectively. Therefore, by using the MoS_2 ALE process, one monolayer MoS_2 could be removed without damaging the exposed MoS_2 layer, and the mobility difference between the exfoliated monolayer MoS_2, monolayer MoS_2 after 1 cycle ALE, and monolayer MoS_2 overexposed after the 1 cycle ALE seems to be in the error range in the fabrication of the different FETs.

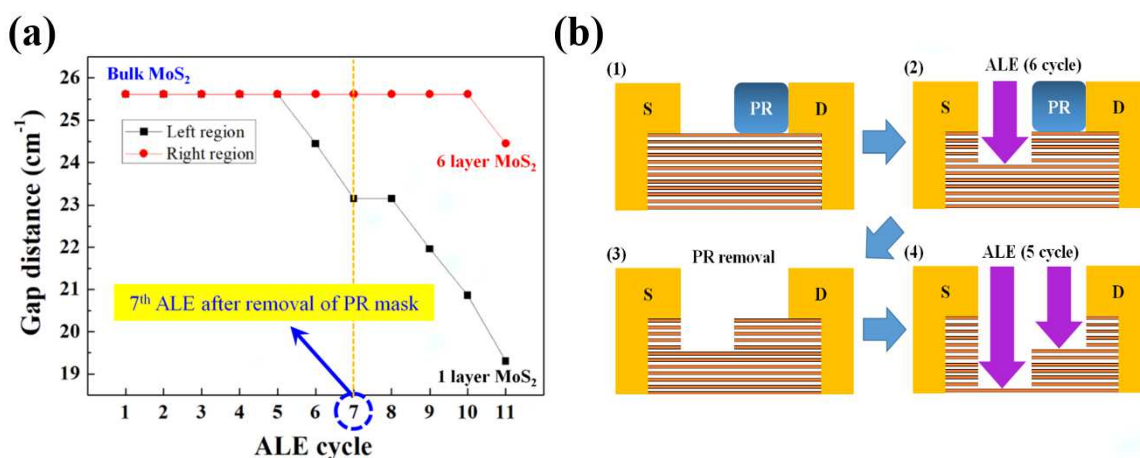

Figure 4. Fabrication of mono-/multi-layer lateral-heterojunction structures by selective ALE process after photoresist (PR) masking on the bulk MoS_2. (a) Raman gap distance change with selective ALE process on the bulk MoS_2 and (b) schematic diagram of the mono-/multi-layer lateral heterojunction fabrication process.

Downloaded on 2018-12-06 to IP 203.252.59.115 address. Redistribution subject to ECS terms of use (see ecsdl.org/site/terms_use) unless CC License in place (see abstract).

Figure 4 show the fabrication process of the mono-/multi-layer lateral-heterojunction structure by selective ALE process after the PR masking with the bulk MoS_2 using photolithography process. Figure 4(a) shows the gap distance change of E^1_{2g} peak and A_{1g} peak of the Raman spectroscopic data according to the number of ALE processes. The 6 cycles ALE process was performed on the left region exposed in the bulk MoS_2 and the layer was reduced from the bulk MoS_2 to multi-layer MoS_2 (in this case, 6 layer MoS_2) through the gap distance decrease from 25.6 to 23.3 cm^{-1}. Then, the right region was opened by removing the PR mask before the 7th ALE process, and an additional ALE cyclic process (in this case, 5 cycles) was performed until the left region MoS_2 becomes a mono-layer. Figure 4(b) shows a schematic diagram of the process of fabricating the mono-/multi-layer lateral-heterojunction structure from a bulk MoS_2 and, using this heterojunction MoS_2 structure, excellent MoS_2 device properties could be obtained (will discussed later). It is believed that the fabrication of the mono-/multi-layer lateral-heterojunction MoS_2 structure using the selective ALE technology can be a very important technique for various TMD materials for the next-generation nanodevices as well as MoS_2 which have different band-gap characteristics depending on the number of layers.

Acknowledgments

This work was supported by the Nano-Material Technology Development Program through the National Research Foundation of Korea (NRF), funded by the Ministry of Education, Science and Technology (2016M3A7B4910429).

References

1. Jeon, J. et al. *Nanoscale*, **7**, 1688 (2015).
2. Dumcenco, D. et al. *ACS Nano* **9**, 4611 (2015).
3. Kim, H. et al. *ECS Trans.* **58**, 47 (2013).
4. Eda, G. et al. *Nano Lett.* **11**, 5111 (2011).
5. Liu, Y. et al. *ACS Nano*, **7**, 4202 (2013).
6. Huang, Y. et al. *Nano Res.*, **6**, 200 (2013).
7. Castellanos-Gomez, A. et al. *Nano Lett.*, **12**, 3187 (2012).
8. Lu, X. et al. *Nanoscale* **5**, 8904 (2013).
9. Wu, J. et al. *Small* **9**, 3314 (2013).
10. Kim, K. S. et al. *ACS Appl. Mater. Interfaces*, **9**, 11967 (2017).
11. Kim, K. S. et al. *Sci. Rep.* **7**, 2462 (2017).

Downloaded on 2018-12-06 to IP 203.252.59.115 address. Redistribution subject to ECS terms of use (see ecsdl.org/site/terms_use) unless CC License in place (see abstract).